Theor Chem Acc (2010) 126:39–44
DOI 10.1007/s00214-009-0672-3

REGULAR ARTICLE

DFT study of the electronic, vibrational, and optical properties of SnO_2

Pablo D. Borges · Luisa M. R. Scolfaro · Horácio W. Leite Alves · Eronides F. da Silva Jr.

Received: 12 October 2009 / Accepted: 21 October 2009 / Published online: 10 November 2009

Abstract We report results on the electronic, vibrational, and optical properties of SnO_2 obtained using first-principles calculations performed within the density functional theory. All the calculated phonon frequencies, real and imaginary parts of complex dielectric function, the energy-loss spectrum, the refractive index, the extinction, and the absorption coefficients show good agreement with experimental results. Based on our calculations, the SnO_2 electron and hole effective masses were found to be strongly anisotropic. The lattice contribution to the low-frequency region of the SnO_2 dielectric function arising from optical phonons was also determined resulting the values of $\varepsilon_{1\perp}^{\text{latt}}(0) = 14.6$ and $\varepsilon_{1\parallel}^{\text{latt}}(0) = 10.7$ for directions perpendicular and parallel to the tetragonal c-axis, respectively. This is in excellent agreement with the available experimental data. After adding the electronic contribution to the lattice contribution, a total average value of $\varepsilon_1(0) = 18.2$ is predicted for the static permittivity constant of SnO_2.

Keywords Density functional calculations · Electronic structure · Effective masses · Phonons · Dielectric permittivity · Optical properties · SnO_2

1 Introduction

Tin dioxide (SnO_2), known also as stannic oxide or cassiterite, is a key functional material in many applications, such as transparent conducting electrodes, solar cells, and gas sensors. As a compound with a wide band gap ($E_g = 3.6$ eV) [1] and high-dielectric constant (high-k), SnO_2 is also of general interest for the next generation gate oxides for Si-based electronic devices [2, 3]. Owing to the fact that the oxide can relatively easily be doped, appropriate conduction band offset with Si may be achieved. Moreover, SnO_2 is also a potential candidate for applications in optoelectronics, such as in light emitting diodes, laser diodes, etc.

Although SnO_2 has been studied for more than three decades, the existing reported results on its electronic structure, vibrational modes, and related properties are still incomplete [4–10]. A few years ago, Mäki-Jaskari and Rantala [9] had calculated the band structure, the energy dependence of both the electronic contribution of the real and imaginary parts of the dielectric function and the optical absorption of SnO_2. However, instead of correlating their results to the high values of the dielectric constant exhibited by this material [2, 11], their data were used only to interpret their evaluated dielectric function and optical

P. D. Borges · L. M. R. Scolfaro
Instituto de Física, Universidade de São Paulo,
C.P. 66318, São Paulo, SP 05315-970, Brazil
e-mail: pdborges@gmail.com

Present Address:
L. M. R. Scolfaro (✉)
Department of Physics, Texas State University, San Marcos,
TX 78666, USA
e-mail: scolfaro@if.usp.br; ls61@txstate.edu

H. W. Leite Alves
Departamento de Ciências Naturais, Universidade Federal de
São João Del Rei, C.P. 110, São João Del Rei,
MG 36301-160, Brazil
e-mail: hwlalves@ufsj.edu.br

E. F. da Silva Jr.
Departamento de Física, Universidade Federal de Pernambuco,
Recife, PE 50670-901, Brazil
e-mail: eron@ufpe.br

absorption of the SnO_2 (110) surfaces, which was described in this same paper.

From the vibrational properties point of view, Parlinski and Kawazoe [10] have calculated the phonon dispersion and the Grüneisen parameters for the zone center modes of SnO_2. Despite the fact that the results they obtained are in good agreement with the known experimental data, their evaluated LO modes at Γ were obtained by extrapolation of the LO branch obtained at points close to Γ, due to the fact that they did not include linear response effects in their calculations. Moreover, for the same reasons, Z^* and $\varepsilon_1(0)$ were only approximately calculated. They also did not take into account the SnO_2 lattice asymmetry that, in the rutile structure, results in the c lattice vector, which is not having the same value as a and b (with $a = b$). In our calculations, we distinguish the parallel and perpendicular components of these tensors.

Until recently, there are no studies reporting theoretical values for SnO_2 carrier effective masses, as well as for some of its optical properties and effective charges that can be directly compared with experiment. In our previous work [12], by using the full-potential linear augmented plane-wave (FP-LAPW) within a full-relativistic approach and by including the spin–orbit coupling effects, we have shown that the effective masses are highly anisotropic, with the holes heavier than the electrons. Moreover, we have shown that the electronic part of the dielectric constant are $\varepsilon_{1\perp}(0) = 4.5$ and $\varepsilon_{1\parallel}(0) = 4.8$, and for our evaluated refraction indexes $n_{\perp}(0)$ and $n_{\parallel}(0)$, we obtained the values of 2.15 and 2.20, respectively, which compares well with the available experimental data.

However, there are no previous attempts to derive the static permittivity constant of SnO_2 using computing methods which consider both the bare electronic contribution as well as the lattice contribution arising from the transversal optical phonons which are important for the correct evaluation of the $\varepsilon_1(0)$ in this class of compounds, as shown recently for HfO_2 [13].

In the present work, we address the above issue and provide detailed calculations of energy-dependent optical properties, such as the real and imaginary parts of the complex dielectric function, the energy loss-function, the refractive index, the extinction and the absorption coefficients, phonon vibrational modes, Born effective charges, as well as the electron and hole effective mass values for SnO_2 as obtained using ab initio theoretical methods, completing the information described in our previous results [12]. The obtained phonon frequencies show good accordance with the available experimental results. In addition, the calculated value for the SnO_2 static dielectric constant, $\varepsilon_1(0)$, is in excellent agreement with the experimental data showing that the vibrational contribution to ε_1 is the origin of the high-k feature of SnO_2.

2 Theoretical methods

Our calculations for crystalline SnO_2 in the rutile (r-) structure were based on the density functional theory in the generalized gradient approximation for the exchange-correlation term (DFT-GGA) [14, 15] according to Perdew–Burke–Ernzerhof [16]. The electron–ion interaction was described by pseudopotentials generated within the Projector-Augmented Wave (PAW) scheme [17, 18], as implemented in the Vienna Ab-initio Simulation Package (VASP-PAW) [19, 20], and the scalar relativistic contributions plus the spin–orbit (*so*) interaction were included in the calculations.

The PAW method allows for the accurate treatment of the Sn 4*d*, 5*s*, and 5*p* electrons, and the O 2*s* and 2*p* electrons which were treated as part of the valence band states. The inclusion of the *so* corrections are found to play a role only in the Sn4*d*-derived states, and consequently on the Sn4*d*–O2*s* interaction due to the splitting of the *d*-levels, and neither affect the highest valence band (VB) states nor the lowest conduction band (CB) states. Values of carrier effective masses are found to change by less than one percent, therefore, the *so* effects will be neglected in the results shown here.

We have also used both DFT-LDA and DFT-GGA, together with the pseudopotential method ABINIT [21] in order to calculate the vibrational spectra of r-SnO_2 to evaluate the phonon frequencies, Born effective charges and the transversal optical phonon contribution to the static permittivity constant. For this, we followed the recipe recently discussed in Ref. [13], where the phonon spectra were obtained using density-functional perturbation theory, as also described in Ref. [22].

3 Results

The equilibrium structure of the r-SnO_2 was obtained by relaxing its unit cell with respect to the lattice parameters a, c, and internal parameter u. We obtained values $a = 4.839$ Å, $(c/a) = 0.670$, and $u = 0.306$, which are in good agreement with the experimental data [23], and also with other ab initio results [7, 8, 12, 24].

The band structure of r-SnO_2 along high-symmetry axis of the crystal Brillouin zone (BZ) is displayed in Fig. 1, together with the projected density of states (PDOS). A direct band gap at Γ of 0.65 eV (0.60 eV if the Sn 4*d* electrons are frozen in the core) is obtained. This feature is in agreement with that observed in our previous report by using the FP-LAPW method with relativistic corrections [12]. The treatment of the Sn(4*d*) electrons as valence band electrons is responsible for a hyperdeep band lying around 21 eV below the VB maximum. X-ray photoemission

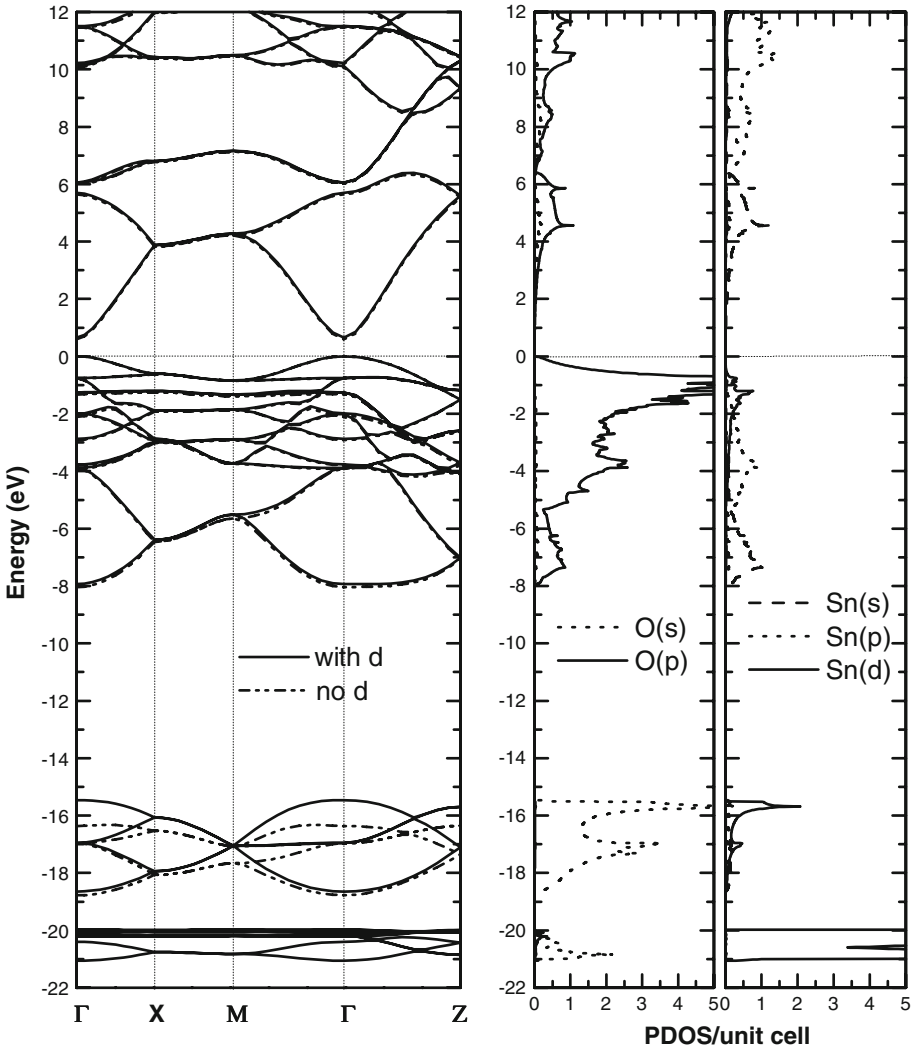

Fig. 1 Band structure of SnO_2 along high-symmetry axis of the BZ (*left panel*) and projected density of states (PDOS) (*two right panels*). The energy zero (*horizontal short-dot line*) was set at the VB maximum

spectroscopy data show this band has to be located at ≈21.5 eV, with respect to the main peak which is due to O(*p*) states close to the top of the VB [25]. We may point out that, as observed for other oxides and nitrides, such as in e.g. ZnO and InN, the well known underestimated O(*p*)—metal(*d*) repulsion observed [26], occurs also for SnO_2, although in the latter case, it is smaller due to the deeper position in the VB of the Sn(4*d*), when compared to that of Zn(3*d*) and In(4*d*). The top of the VB mostly consists of contributions from the O(*p*) states, while the bottom of the CB has an anti-bonding character arising from the Sn(4*s*) and O(*p*) states.

Table 1 depicts the calculated values for the carrier effective masses in the $\Gamma \rightarrow M$, $\Gamma \rightarrow X$, and $\Gamma \rightarrow Z$ directions of the BZ. We observe that the carrier effective masses in SnO_2 are very anisotropic, as indicated qualitatively in our previous work [12]. Our predicted values for the electron effective mass, the perpendicular ($\perp$) and parallel ($\|$) components with respect to the tetragonal *c* axis, may be compared with the experimental values which in general

Table 1 Electron (m^*_e) and hole (m^*_h) effective masses for SnO_2 in units of m_0 (the free electron mass) along high-symmetry directions in the BZ

	m^*_e	m^*_h
$\Gamma \rightarrow X$	0.48	3.241
$\Gamma \rightarrow M$	0.48	3.337
$\Gamma \rightarrow Z$	0.192	2.263

show values spreading between 0.1 and 0.8 m_0 [27]. While anisotropy has been indicated $m^*_{e\perp} = 0.299\ m_0$ and $m^*_{e\|} = 0.234\ m_0$ from cyclotron resonance measurements [28], this is not as large as we predict. A good agreement between the value of $m^*_e = 0.4\ m_0$ [29] and our theoretical calculation is observed if we consider the calculated isotropic effective mass, given by $m^*_e = (2m^*_{e\perp} + m^*_{e\|})/3 = 0.38\ m_0$. To our knowledge, there is no experimental data reported for holes effective masses in SnO_2.

From the electronic structure calculations, we have obtained the imaginary part, $\varepsilon_2(\omega)$, of the complex

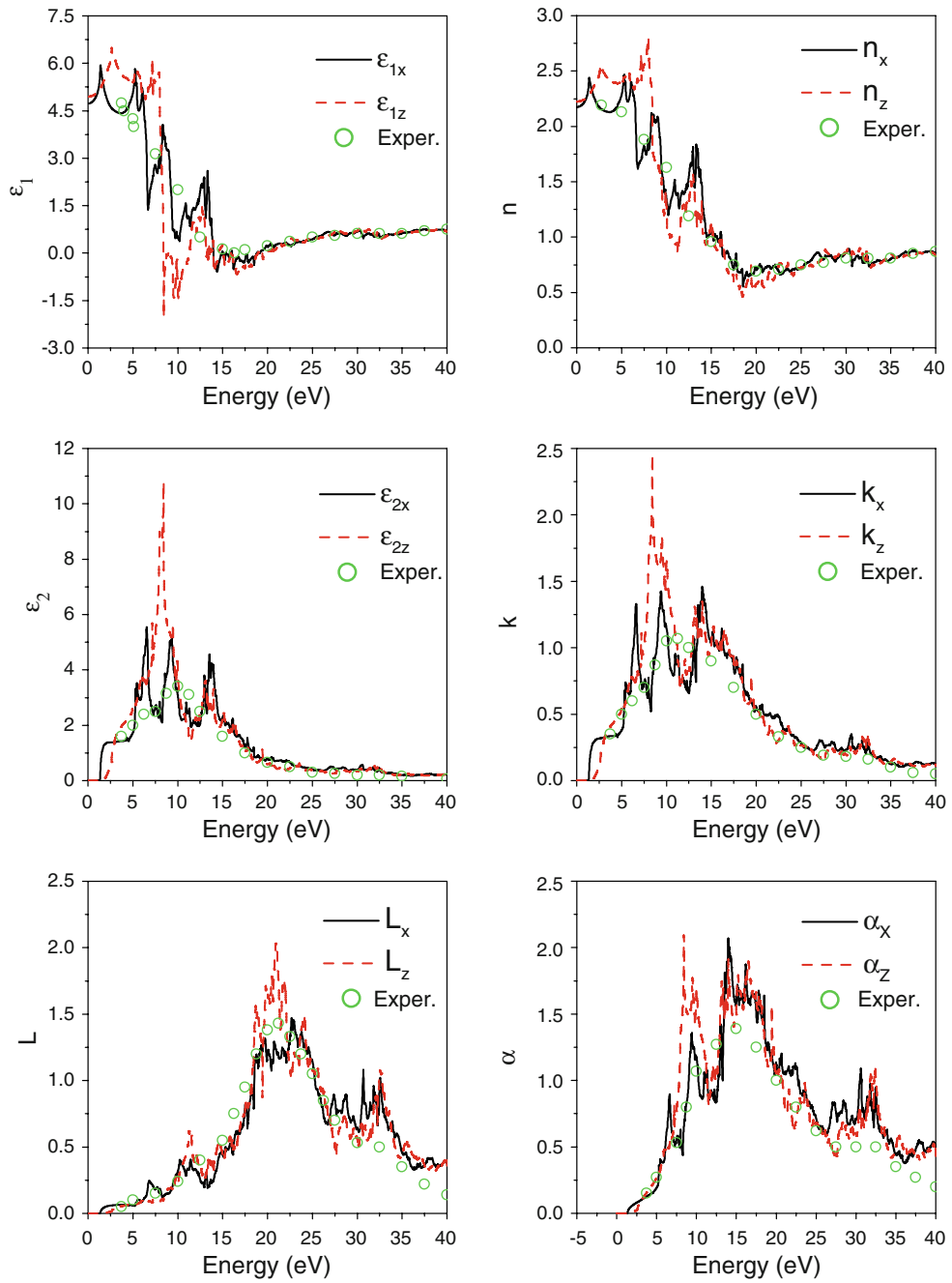

Fig. 2 *Left panels*: Energy-dependent real (ε_1) and imaginary (ε_2) parts of the SnO_2 dielectric function, as well as the energy-dependent loss-energy function (L). *Right panels*: Energy-dependent refractive index (n), and the energy-dependent extinction (k) and absorption (α) coefficients. Experimental data, shown by *open circles*, correspond to results obtained using reflection electron energy loss spectroscopy (REELS) measurements and were extracted from Ref. [30]

dielectric function directly from the VASP code, and then have used the Kramers–Kronig relation to get its real part, $\varepsilon_1(\omega)$. Figure 2 depicts the energy-dependent ε_1 and ε_2, as well as the loss-energy function L, the refractive index n, the extinction and absorption coefficients. Some anisotropy is seen for all calculated optical properties for energies lower than 15 eV with the exception of the loss-energy function, L, and of the absorption coefficient α which are anisotropic in the energy range 10–40 eV. The theoretical curves are in excellent agreement with the experimental data (shown as open circles in the figure), as obtained from reflection electron energy loss spectroscopy (REELS) measurements carried out between 4 and 40 eV [30].

An average value of $\varepsilon_1(0) = 4.95$ is calculated for the *electronic* contribution to the static dielectric constant, in

Table 2 Evaluated zone-center phonon frequencies (cm^{-1}) for SnO_2 compared with the available experimental data (taken from Refs. [32, 33]) and other theoretical results (taken from Ref. [10])

Mode	LDA	GGA	Experimental	Theoretical
B_{1g}	82.58	90.24	87–123	104.7
B_{1u}	138.4	133.7	–	146.8
E_u(TO)	200.3	196.5	244.0	241.5
E_u(LO)	251.9	237.1	276.0	278.9
E_u(TO)	270.5	253.3	293.0	285.9
E_u(LO)	306.9	294.0	366.0	406.3
A_{2g}	320.3	314.2	–	366.3
A_{2u}(TO)	457.4	424.2	477.0	461.0
E_g	462.4	432.6	472–476	469.7
B_{1u}	552.6	519.7	–	585.1
E_u(TO)	584.1	538.0	618.0	581.4
A_{1g}	617.3	577.6	632–638	638.1
A_{2u}(LO)	648.5	606.9	705.0	657.1
E_u(LO)	711.8	662.3	770.0	703.5
B_{2g}	733.8	688.2	773–782	761.9

accordance with previous ab initio studies of r-SnO_2 [4]. The value we obtained for the refractive index $n(0) = 2.2$ is also in good agreement with reported data [31].

By using the ABINIT code, we were able to calculate the phonon spectra of r-SnO_2, and the calculated zone-center phonon frequencies (cm^{-1}) are depicted in Table 2. The corresponding phonon dispersion was already published in our previous work [11]. The results obtained are in good agreement with the available experimental data. The same holds for the comparison with the other theoretical calculations except for the second E_u(LO) mode, where the observed difference must be a consequence of the extrapolation method used in Ref. [10]. Here, we have performed a full lattice dynamics calculations which includes not only the harmonic terms, but also those terms which come from the long range Coulomb interactions as obtained by the Linear Response calculations implemented in the ABINIT code [21].This was not done in the previous theoretical work. Finally, we would also like to remark that LDA calculations tend to underestimate the phonon frequencies due to an overestimation of the obtained bulk modulus, as verified in our previous work [11], while for the GGA ones, the opposite occurs.

Concerning the lattice asymmetry of the rutile structure, DFT-LDA values we obtained for the Born effective charges of r-SnO_2 are

$$Z^*(Zr) = \begin{pmatrix} 4.20 & 0.54 & 0.00 \\ 0.54 & 4.20 & 0.00 \\ 0.00 & 0.00 & 4.62 \end{pmatrix},$$

and

$$Z^*(O) = \begin{pmatrix} -2.09 & -0.77 & 0.00 \\ -0.77 & -2.09 & 0.00 \\ 0.00 & 0.00 & -2.31 \end{pmatrix},$$

which, besides the natural difference between the c (the parallel component) and both a and b lattice vectors (the perpendicular ones), there is some degree of anisotropy of the effective charges in the perpendicular direction, due to non-zero values obtained for the non-diagonal terms of these tensors. Comparing values we obtained for the Born effective charges with those previously calculated, we infer that calculations using extrapolation of the LO branches, as those done by Parlinski and Kawazoe [10], give rough results for both Z^* and $\varepsilon_1(0)$. However, their results can be used as an initial guess for obtaining the true values of these properties. In addition, we would like to remark that DFT-GGA values determinated for the Born effective charges of r-SnO_2 are similar to the DFT-LDA ones, and they are around 1% higher.

With the knowledge of the TO frequencies, we then evaluate the phonons' contribution to the low-frequency region of the frequency-dependent dielectric function. Figure 3 shows the results for the perpendicular ($\perp$) and parallel ($\|$) components of ε_1 and ε_2, named ε_{1x}, ε_{2x}, and ε_{1z}, ε_{2z}, respectively, together with a fitting by means of the Lorentz–Drude model. Specifically, we use the following expressions

$$\varepsilon_1(\omega) = \varepsilon_1(\infty) + \sum_{i=1}^{m} \frac{\omega_{pi}^2(\omega_{TOi}^2 - \omega^2)}{[(\omega_{TOi}^2 - \omega^2)^2 + \gamma_i^2\omega^2]}, \quad (1)$$

$$\varepsilon_2(\omega) = \sum_{i=1}^{m} \frac{\gamma_i\omega_{pi}^2\omega_{TOi}}{[(\omega_{TOi}^2 - \omega^2)^2 + \gamma_i^2\omega^2]}, \quad (2)$$

where m is the total number of oscillators, ω_{pi} is the plasmon frequency for ith oscillator, and γ_i is its damping parameter, which is directly related to sample size.

For both the $\varepsilon_{1\perp}(\omega)$ and $\varepsilon_{2\perp}(\omega)$, three E_u modes, at 200.2, 270.6 and 584.5 cm^{-1} with their plasmon frequencies of 535.1, 220.1 and 826.3 cm^{-1}, respectively, were necessary for the fitting, with a fixed value for γ of 0.01. For the parallel component, only A_{2u} at 457.7 cm^{-1} with the plasmon frequency of 1,060.7 cm^{-1} was necessary, and we kept γ fixed with the same value used in the perpendicular direction.

The values $\varepsilon_{1\perp}^{\text{latt}}(0) = 14.6$ and $\varepsilon_{1\|}^{\text{latt}}(0) = 10.7$ were obtained for directions perpendicular and parallel to the tetragonal c-axis, respectively, in excellent agreement with the available experimental data obtained from far-infrared spectroscopy data, 14.2 ± 2 and 9.0 ± 0.5 [34], and also with the measured average value of 12.5 reported in Ref. [35].

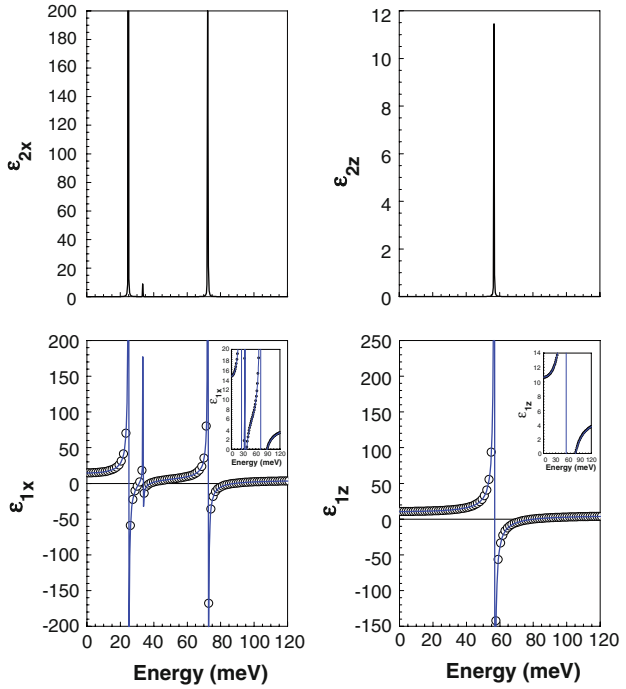

Fig. 3 Calculated energy-dependent real (*bottom*) and imaginary (*top*) parts of the ⊥ and ∥ components of the lattice contribution for the low-energy region of the dielectric function of SnO_2, fitted by the Drude–Lorentz equation for m oscillators ($m = 3$ and $m = 1$ for the ⊥ and ∥ cases, respectively)

4 Conclusions

In summary, results for electronic, vibrational, and optical properties of SnO_2 based on ab initio calculations performed within density functional theory were presented. By combining the calculated lattice contributions to the static dielectric constant with its electronic part, an average value of $\varepsilon_1(0) \sim [(2 \times \varepsilon_{1\perp}^{\text{latt}}(0) + \varepsilon_{1\parallel}^{\text{latt}}(0))/3] + 4.95 = 18.2$ is predicted for the static permittivity constant of SnO_2. This allows us to conclude that low-frequency optical phonons are the primary contributors to the high-k value observed for tin dioxide. The calculated optical phonons as well as the energy-dependent optical quantities, real and imaginary parts of complex dielectric function, the energy-loss, the refractive index, the extinction and the absorption coefficients are in good agreement with the experimental available data. Strongly anisotropic electron and hole effective masses are also predicted. Our predictions will certainly be of relevance in future analysis and design of new SnO_2-based nanostructures devices.

Acknowledgments We thank Friedhelm Bechstedt from Jena University, Germany, and Thomas H. Myers from Texas State University, USA, for critical reading of the manuscript. The authors also acknowledge the support received from the Brazilian research financial agencies CAPES and CNPq (grants 550.126/05-8/CTPETRO, 303.817/05-4/PQ and 301.697/07-8/PQ).

References

1. Batzill M, Diebold U (2005) Prog Surf Sci 79:47
2. Robertson J (2006) Rep Prog Phys 69:327
3. Kiliç C, Zunger A (2002) Phys Rev Lett 88:095501
4. Mi Y, Odaka H, Iwata S (1999) Jpn J Appl Phys 38:3453
5. Robertson J, Xiong K, Clark SJ (2006) Thin Solid Films 496:1
6. Robertson J (1979) J Phys C Solid State Phys 12:4767
7. Peltzer y Blancá EL, Svane A, Christensen NE, Rodrigues CO, Cappannini OM, Moreno MS (1993) Phys Rev B 48:15712
8. Duan Y (2008) Phys Rev B 77:045332
9. Mäki-Jaskari MA, Rantala TT (2001) Phys Rev B 64:075407
10. Parlinski K, Kawazoe Y (2000) Eur Phys J B13:679
11. Leite Alves HW, Silva CC, Lino AT, Borges PD, Scolfaro LMR, da Silva EF Jr (2009) Appl Surf Sci 255:752
12. Lino AT, Borges PD, Scolfaro LMR, Rodrigues SCP, da Silva EF Jr (2007) In: Jantsch W, Schäffler F (eds) AIP conference proceedings, vol 893. AIP, Melville, pp 259–260
13. Garcia JC, Scolfaro LMR, Lino AT, Freire VN, Farias GA, Silva CC, Leite Alves HW, Rodrigues SCP, da Silva EF Jr (2006) J Appl Phys 100:104103
14. Hohemberg P, Kohn W (1964) Phys Rev 136:B864
15. Kohn W, Sham LJ (1965) Phys Rev 140:A1133
16. Perdew JP, Burke K, Ernzerhof M (1996) Phys Rev Lett 77:3865
17. Kresse G, Joubert D (1999) Phys Rev B 59:1758
18. Adolph B, Futhmüller J, Bechstedt F (2001) Phys Rev B 63:125108
19. Kresse G, Futhmüller J (1996) Comput Mater Sci 6:15
20. Kresse G, Futhmüller J (1996) Phys Rev B 54:11169
21. Gonze X, Beuken J-M, Caracas R, Detraux F, Fuchs M, Rignanese G-M, Sindic L, Verstraete M, Zerah G, Jollet F, Torrent M, Roy A, Mikami M, Ghosez P, Raty J-Y, Allan DC (2002) Comput Mater Sci 25:478
22. Gonze X, Lee C (1997) Phys Rev B 55:10355
23. Wyckoff RWG (1963) Crystal structures, 2nd edn. Interscience, New York, p 251
24. Meyer M, Onida G, Palummo M, Reining L (2001) Phys Rev B 64:045119
25. Themlin J-M, Chtaïb M, Henrard L, Lambin P, Darville J, Gilles J-M (1992) Phys Rev B 46:2460
26. Schleife A, Fuchs F, Furthmüller J, Bechstedt F (2006) Phys Rev B 73:245212
27. Jarzebski ZM, Marton JP (1976) J Electrochem Soc 123:299C
28. Button KJ, Fonstad CG, Dreybrodt W (1971) Phys Rev B 4:4539
29. Rakhshani AE, Makdisi Y, Ramazaniyan HA (1998) J Appl Phys 83:1049
30. Yubero F, Jiménez VM, González-Elipe AR (1998) Surf Sci 400:116
31. Chatelon JP, Terrier C, Roger JA (1999) Semicond Sci Technol 14:642
32. Katiyar RS, Dawson P, Hargreave MM, Wilkinson GR (1971) J Phys C Solid State Phys 4:2421
33. Peercy PS, Morosin B (1973) Phys Rev B 7:2779
34. van Daal HJ (1968) J Appl Phys 39:4467
35. Works CN (1947) J Appl Phys 18:605